Undetected Minority-polarity Flux as the Missing Link in Coronal Heating

Y.-M. Wang

Space Science Division, Naval Research Laboratory, Washington, DC 20375, USA

yi.wang@nrl.navy.mil

ABSTRACT

During the last few decades, the most widely favored models for coronal heating have involved the in situ dissipation of energy, with footpoint shuffling giving rise to multiple current sheets (the "nanoflare" model) or to Alfvén waves that leak into the corona and undergo dissipative interactions (the wave heating scenario). As has been recognized earlier, observations suggest instead that the energy deposition is concentrated at very low heights, with the coronal loops being filled with hot, dense material from below, which accounts for their overdensities and flat temperature profiles. While an obvious mechanism for footpoint heating would be reconnection with small-scale fields, this possibility seems to have been widely ignored because magnetograms show almost no minority-polarity flux inside active region (AR) plages. Here, we present further examples to support our earlier conclusions (1) that magnetograms greatly underrepresent the amount of minority-polarity flux inside plages and "unipolar" network, and (2) that small loops are a major constituent of Fe IX 17.1 nm moss. On the assumption that the emergence or churning rate of small-scale flux is the same inside plages as in mixed-polarity regions of the quiet Sun, we estimate the energy flux density associated with reconnection with the plage fields to be on the order of 10^7 erg cm^{-2} s^{-1}, sufficient to heat the AR corona.

Keywords: Active Regions, Magnetic Fields; Heating, Coronal; Magnetic Fields, Corona; Magnetic Fields, Photosphere; Magnetic Reconnection, Observational Signatures

1. INTRODUCTION

Coronal heating models are generally of two kinds: those that invoke magnetohydrodynamic (MHD) waves and their dissipation, and those that rely more directly on magnetic

reconnection or the formation of current sheets (see, e.g., Parnell and De Moortel, 2012, and references therein). In both cases, footpoint motions are usually taken to be the driving force and granular convection the basic energy source. Although it is possible (and even likely) that both wave dissipation and reconnection are involved in coronal heating, there is no consensus as to which process is the dominant one.

Alfvén waves generated at the photosphere are strongly reflected due to the steep falloff of the density and increase in the Alfvén speed with height, and only a very small fraction of the wave energy leaks through the transition region into the corona (see, e.g., Cranmer and Ballegooijen, 2005). Given the presence of a sufficiently large wave flux density in the corona, the mechanisms by which the Alfvén waves are dissipated (resonant excitation, phase mixing, turbulent interactions between outgoing and reflected waves) continue to be debated (see, e.g., De Groof and Goossens, 2002; Howson et al., 2019; van Ballegooijen et al., 2014).

Heating by reconnection has been well observed in flares and jets, on scales ranging from X-ray and extreme-ultraviolet (EUV) bright points (and the "campfires" discovered by *Solar Orbiter*: Berghmans et al., 2021) to active regions (ARs). In the well-known nanoflare model of Parker (1988), random footpoint motions spontaneously give rise to tangential discontinuities/current sheets in the coronal field, leading to multiple reconnection events ("nanoflares") and ohmic dissipation (for a recent discussion of this model, see Pontin and Hornig, 2020). One possible difficulty with this scenario is that the upper parts of coronal loops generally appear smooth and featureless, seemingly inconsistent with the large departures from a potential field that would be associated with the predicted magnetic braiding (van Ballegooijen et al., 2011). As emphasized by Aschwanden et al. (2007), it is at the footpoints of coronal loops that topologically complex structures are observed. They also argued that the high densities in AR loops and the absence of large temperature gradients along them can only be explained if the corona is not heated locally but from below, via chromospheric evaporation.

It has previously been suggested that small bipoles or ephemeral regions (ERs) are the main source of coronal heating in the quiet Sun (Schrijver et al., 1998) and in coronal holes (Parker, 1991). However, a strong argument against reconnection with small-scale fields playing a major role in heating coronal holes and the AR corona was provided by the statistical study of ERs by Hagenaar et al. (2008, 2010). From an examination of *Michelson Doppler Interferometer* (MDI) magnetograms recorded during 2000–2005, they concluded that the rate of ER emergence is at least a factor of 3 smaller inside predominantly unipolar areas than in regions where the polarities are more mixed. This reduction is too large to be attributed to the shorter cancellation timescales of minority-polarity flux in a strongly unipolar background.

In their analysis of continual intermittent outflow observed in AR loops with the *Transition Region and Coronal Explorer* (TRACE), Winebarger et al. (2001) conjectured that the flows were driven by small-scale reconnection events, but found no evidence for underlying flux cancellation in MDI magnetograms. Similarly, Aschwanden et al. (2007) mentioned as a "caveat" against the chromospheric evaporation scenario "the nondetection of the initial heating agent (small-scale reconnection events in the transition region)". More recently, in their observational study of the relation between magnetic structures and signatures of heating in a plage region, Anan et al. (2021) found that the fraction of opposite-polarity fields was too small to support reconnection mechanisms, except possibly in the "strong guide-field regime."

However, we have recently come to question the reliability of present-day magnetograms in detecting minority-polarity flux in the presence of a strongly dominant polarity. In an analysis of coronal EUV plumes employing data from the *Atmospheric Imaging Assembly* (AIA) and *Helioseismic and Magnetic Imager* (HMI) on the *Solar Dynamics Observatory* (SDO), Wang et al. (2016) found that strong plume emission sometimes occurred above network concentrations that were purely unipolar according to the HMI magnetograms, but the corresponding AIA images clearly showed small, looplike structures in the cores of the plumes. In subsequent studies focusing on unipolar plage areas, Wang (2016) and Wang et al. (2019) identified large numbers of looplike features embedded within the plages, some having the inverted-Y topology characteristic of jets. The footpoint structures had horizontal extents of $\sim 2''$–$7''$ ($\sim$1.5–5 Mm), greatly exceeding the HMI pixel size of $0.5''$; the absence of corresponding minority-polarity signatures thus appears to be related to the magnetograph's sensitivity to weak signals when one polarity is heavily dominant, and not simply the result of inadequate spatial resolution.

Analyzing $\sim 0.1''$-resolution measurements of an emerging AR from the *SUNRISE Imaging Magnetograph Experiment* (IMaX), Chitta et al. (2017) found that the footpoints of coronal loops were often located near minority-polarity flux that was invisible or barely visible in the corresponding lower-resolution HMI magnetograms. However, the minority-polarity elements detected with IMaX were confined to the edges of the strong plage areas, whereas the small looplike features identified in Wang (2016) and Wang et al. (2016, 2019) were located well inside the supposedly unipolar plages and network concentrations, as well as at their peripheries.

In this paper, we describe more examples of looplike features and compact brightenings at the footpoints of AR loops embedded in "unipolar" plages, and discuss the nature and origin of the small loops and their relationship to AR moss. We then argue that they provide an energy flux sufficient to heat the AR corona.

2. The Energization of AR Loops by Footpoint Reconnection: SDO Observations

The AIA instrument records full-disk images in seven EUV channels, with 0.6″ pixels and 12 s cadence, as well as in two UV and a white-light channel. HMI provides line-of-sight magnetograms every 45 s, with a noise level of ∼10 G. For this study, we employ AIA images taken in three passbands: 17.1 nm, dominated by Fe IX ($T \sim 0.7$–0.8 MK), 19.3 nm, dominated by Fe XII ($T \sim 1.5$–1.6 MK), and 21.1 nm, dominated by Fe XIV ($T \sim 1.9$–2.0 MK). The AIA and HMI images were coaligned using the IDL procedures *read_sdo* and *aia_prep* from the SolarSoft library.

2.1. NOAA 12443: 2015 November 5

As our first illustrative example, Figure 1 shows an evolving collection of AR loops inside NOAA 12243, as they appear in the 17.1 and 19.3 nm passbands late on 2015 November 5. The loops are rooted in purely positive-polarity plage according to the magnetograms in the rightmost column. As seen most clearly in the 17.1 nm images, small, curved structures with dimensions of a few arcseconds are present at and around the footpoints of the longer loops. The looplike fine structure appears to be an integral part of the 17.1 nm moss that overlies the plage area. The intensity of the reticulated moss shows substantial spatial variations, being considerably brighter inside the circled area and in the foreground of the images than in the intervening region, which is partially covered by dark filamentary material. The footpoint structures and the overlying emission are also visible in the 19.3 nm images, but are much more diffuse.

The reticulated, spongy morphology of the 17.1 nm moss is partly due to the presence of cool chromospheric jets (De Pontieu et al., 1999, 2009), which may take the form of "dynamic fibrils," mottles, and/or spicules (see, e.g., Hansteen et al., 2006; Tsiropoula and Tziotziou, 2004); these inclusions give rise to the dark "holes" seen in the moss. In some cases, a curved feature appearing at the base of an AR loop may be a projection effect caused by the presence of foreground chromospheric material. However, small, bright, curved structures are visible throughout the moss, and these combine with the dark inclusions to give the moss its reticulated appearance.

2.2. NOAA 12351: 2015 May 23

The small 17.1 nm loops are often more easily discerned when the moss is viewed "at an angle," as when located at relatively high latitudes. Figure 2 shows an area of moss inside a sheared, decaying AR (NOAA 12351) at latitude N22°, as observed on 2015 May 23 in Fe IX (left column) and Fe XII (middle column). A row of looplike features with dimensions of a few arcseconds may be seen, for example, inside the large circle in the 17.1 nm image recorded at 14:00 UTC. Some of these curved structures are embedded within the purely negative-polarity plage, according to the corresponding HMI magnetogram at the far right. However, inside the smaller circle at the southwest corner of the same 17.1 nm image, similar looplike features are also present above a mixed-polarity area at the edge of the plage. This tends to support the conjecture that the small structures inside the plage are indeed loops, but that the magnetograms do not show the minority-polarity inclusions when the majority-polarity flux is strong and heavily dominant. We also note that the morphological similarity between the 17.1 nm fine structure inside and just outside the plage suggests that moss is not confined to plages (see also Figure 10 below).

The small looplike features are also visible in Fe XII 19.3 nm, as near the center of the large circles in the images recorded at 14:00 and 14:30 UTC. This supports the idea that we are observing coronal structures.

2.3. NOAA 12764: 2020 June 6

Figure 3 shows an AR loop system observed at high northern latitudes on 2020 June 6, just after the start of solar cycle 25. Both ends of the loops are embedded in 17.1 nm moss. In the original and sharpened 17.1 nm images, bright, curved features with dimensions of $\sim 5''$ are visible at the eastern ends (circled) of some of the loops; these features seem to be located in purely negative-polarity plage, according to the HMI magnetogram (bottom panel). The 21.1 nm image also shows compact brightenings within this plage area, although their distribution differs from that of the 17.1 nm structures.

2.4. NOAA 12823: 2021 May 13–14

Figure 4 shows the configuration of 17.1 nm loops above a negative-polarity plage area, as it evolves over a period of a day. Again, curved features with dimensions of several Megameters are clearly visible at the base of the AR loops. In this case, however, some of the footpoint loops have at least one leg located above the area of weaker, mixed-polarity

field outside the unipolar plage.

2.5. NOAA 12783: 2020 November 21

In Figure 5, the western end of a bundle of AR loops is viewed "from above" (rather than "from the side" as in the previous examples). The footpoints are located inside an area of negative-polarity plage, and they are again accompanied by looplike fine structure and compact brightenings. Most of these small features appear to lie entirely within the unipolar plage; however, in the 17.1 nm image recorded at 04:14 UTC (bottom left panel), the hook-shaped extension of the AR loops ends in the mixed-polarity region just northward of the plage, as indicated by the corresponding HMI magnetogram (bottom right panel).

Figure 6 shows the western end of another loop system situated just to the north of that in Figure 5. Over a 23 minute period, compact brightenings at the base of the loops give rise to a succession of narrow outflow streams or jets.

2.6. NOAA 12786: 2020 December 2

The sequence of 17.1 nm images in Figure 7 provides another example of continual jet-like activity at the footpoints of AR loops rooted inside or at the edges of unipolar plage areas. The collimated outflows originate from an ever-changing configuration of compact brightenings, some of which are recognizable as small loops.

2.7. NOAA 12791: 2020 December 10

The compact brightenings and jet-like outflows in unipolar plage areas may also be seen at higher temperatures. The sequence of Fe XII 19.3 nm images in Figure 8 illustrates the activity occurring at this location throughout the day. Again, some of the small footpoint features appear to be embedded in flux of a single polarity.

2.8. NOAA 12794: 2020 December 29

The transient loops in Figure 9 are connected to a large, negative-polarity sunspot located to the west of the field of view. The number, width, and intensity of the collimated outflows vary throughout the day. The footpoint areas show complex, looplike fine structure

that is clearly a constituent of the 17.1 nm moss. This fine structure is present even where the underlying flux is weak and of mixed polarity, although most of the salt-and-pepper areas are covered by dark fibrilar material, which dominates the northern half of the 17.1 nm images.

3. Nature of the Footpoint Fine Structure: Ephemeral Regions, Granular Motions, and Moss

According to Fisk (2005), open flux random walks over the solar surface by undergoing interchange reconnection with closed loops, and accumulates in areas where the density of loops is lowest. This prediction was seemingly confirmed by Abramenko et al. (2006), who found that the rate of ER emergence in MDI magnetograms was a factor of 2 lower inside coronal holes than in the quiet Sun, and by Zhang et al. (2006), who found (using magnetograms taken at the Big Bear Solar Observatory) that it was a factor of 3 lower. Subsequently, however, Hagenaar et al. (2008) showed that this reduction applied to unipolar regions in general, not just to coronal holes.

As suggested by the examples of the preceding section, the rate of ER emergence inside AR plages is likely to be much greater than indicated by the magnetograms. Moreover, the looplike fine structure seen in the AIA images appears to be morphologically more or less the same inside and just outside the "unipolar" plage areas, as illustrated by Figure 2, where it is difficult to identify the boundaries between the plage and the surrounding mixed-polarity regions from the 17.1 nm images alone. We therefore infer that the rate of ER emergence is similar inside and outside of unipolar areas, and given by that measured in quiet background regions of the Sun.

The ubiquitous small-scale loops have horizontal extents of $\sim 2''$–$7''$ and lifetimes of a few minutes, which are of the same order as the spatiotemporal scales of the solar granulation ($\sim 2''$ and ∼5–10 minutes). The origin of bipoles with total fluxes $\lesssim 10^{20}$ Mx, including in particular ERs, is often attributed to a poorly understood "surface dynamo" that is separate from the main solar dynamo associated with sunspots and ARs. Harvey et al. (2007; see also Lites et al., 1996) have identified a patchy, nearly horizontal component of the photospheric field with scales ranging from their resolution limit of a few arcseconds to $\sim 15''$. Although they did not observe these "seething" horizontal fields inside ARs and in the magnetic network, we presume that they are also present there but too weak to be detected, just as minority-polarity flux is underdetected in these regions. As for their origin, one possibility is that they are the lingering, widely dispersed remnants of AR fields that have undergone only partial flux cancellation and have not yet fully resubmerged. As shown

in Wang and Berger (2018), the component of the field parallel to the polarity inversion lines of ARs survives many rotations longer than the transverse component. These "axial" fields, which are closely associated with the helicity of ARs, are only canceled/resubmerged after the photospheric neutral lines have themselves been randomized on small scales through flux transport processes (see Figure 7 in Wang and Berger 2018).[1]

The pervasive presence of horizontal fields at or just below the solar surface would provide a source for the small loops and ERs seen in the EUV images. These fields would be continually churned and twisted by the granular convection, and the twisted small-scale fields would continually transfer their energy to the larger coronal loops. As in most models for coronal heating, granular motions are the basic energy source, but instead of acting directly on the AR loops to generate Alfvén waves or tangential discontinuities, the interaction is mediated through the ubiquitous small-scale fields.

In the standard interpretation, moss represents the transition region of hot AR loops (Berger et al., 1999). However, as already noted, comparison of Fe IX 17.1 nm images with magnetograms suggests that moss is not confined to strong plages (see also De Pontieu et al. (1999, 2003), who found that the distribution of moss is poorly correlated with the Ca II K brightness, a proxy for the photospheric field strength). Figure 10 shows another example of moss-like structure overlying a region of relatively weak, mixed-polarity field. In our interpretation, moss consists mainly of small loops that are heated as their magnetic energy is dissipated by interactions with the overlying loops. However, most quiet Sun areas are covered by low-lying 17.1 nm fibrils, which form dark canopies surrounding ARs; these "circumfacular" regions have long been observed at visible wavelengths such as Ca II K (Hale and Ellerman, 1903; St. John, 1911) and Hα (e.g., Howard and Harvey, 1964). As suggested in Wang et al. (2011), the dark fibrils tend to form where the photospheric field is weak and of mixed polarity and the overlying large-scale coronal field has a horizontal orientation, as at the edges of flux concentrations; in this case, reconnection produces cool, dense, low-lying loops which may eventually evolve into filaments.

[1]The axisymmetric (longitude-independent) component of the photospheric field, which is the source of the polar fields, is also extremely long-lived because it is unaffected by differential rotation and decays on the supergranular diffusion timescale. However, this component would not contribute to the relatively small-scale, horizontal background fields in question.

4. Estimating the Contribution of ERs to Coronal Heating in ARs

Following a procedure similar to that applied to coronal holes in Wang (2020), we now estimate the energy flux associated with the emergence of ERs (or the continual churning of horizontal fields) inside AR plages.

We take as our starting point the MDI measurements of Hagenaar et al. (2008, 2010), who found that the rate of ER emergence depended on the flux imbalance parameter $\xi \equiv \Phi_{\rm net}/\Phi_{\rm abs}$, where $\Phi_{\rm net}$ ($\Phi_{\rm abs}$) represents the signed (unsigned) flux summed over a 92×92 Mm^2 area surrounding the ERs. Their result may be expressed as

$$E_{\rm ER}(\xi) \simeq (1.075 - 0.793\xi^2) \times 10^{-3}\ {\rm Mx\ cm^{-2}\ s^{-1}}. \tag{1}$$

The measurements were based on 5 minute averages of line-of-sight magnetograms with 2″ pixels, with the individual ERs having total unsigned fluxes $\Phi_{\rm ER} \gtrsim 4 \times 10^{18}$ Mx.

Based on the discussion of the preceding sections, we assume that the ER emergence rate is the same in unipolar regions and AR plages as in mixed-polarity areas of the quiet Sun, and henceforth set $\xi = 0$. In addition, we apply two further corrections. First, following Tran et al. (2005), who cross-correlated MDI data with saturation-corrected magnetograms from the Mount Wilson Observatory, we scale the measured MDI fluxes upward by a factor of 1.7. Second, we allow for the contribution of ERs with total fluxes down to $\Phi_{\rm ER} \sim 1 \times 10^{18}$ Mx.

The rate of small-scale flux emergence, in the form of ERs and intranetwork flux, is known to exhibit an exponential or power-law dependence that continues to increase toward smaller spatiotemporal scales (see, e.g., Thornton and Parnell, 2011; Zhou et al., 2013). Because our focus is on reconnection events occurring in the corona, we include only the contribution of bipoles whose scale sizes exceed ∼2 Mm. According to Hagenaar (2001), an ER having a total flux of $\Phi_{\rm ER} = 1.13 \times 10^{19}$ Mx (or 1.92×10^{19} Mx when corrected for line profile saturation) has an average pole separation $d_{\rm ER}$ of ∼8.9 Mm. Assuming that $d_{\rm ER} \propto \Phi_{\rm ER}^{1/2}$ (following Cranmer and van Ballegooijen, 2010) and taking the vertical scale size $h_{\rm ER}$ of an ER to be comparable to its pole separation, we may write

$$h_{\rm ER} \sim 2.0\ {\rm Mm}\ \left(\frac{\Phi_{\rm ER}}{1 \times 10^{18}\ {\rm Mx}}\right)^{1/2}. \tag{2}$$

This means that ERs with fluxes $\Phi_{\rm ER} \gtrsim 10^{18}$ Mx will have loop systems that extend to heights above ∼2 Mm, the approximate location of the coronal base.

Although they were unable to extend their ER measurements below fluxes of $\sim 4 \times 10^{18}$ Mx, Hagenaar et al. (2003) showed that the number of emerging ERs as a function of $\Phi_{\rm ER}$

could be fitted with an exponential of the form $N_{\rm ER}(\Phi_{\rm ER}) \propto \exp[-\Phi_{\rm ER}/(5\times10^{18}\ {\rm Mx})]$ (see their Figure 6). Scaling the fluxes upward by 1.7, it follows that

$$E_{\rm ER}(\Phi_{\rm ER} \gtrsim 1\times10^{18}\ {\rm Mx}) \simeq 1.23\ E_{\rm ER}(\Phi_{\rm ER} \gtrsim 6.8\times10^{18}\ {\rm Mx}) \simeq 2.25\times10^{-3}\ {\rm Mx\ cm^{-2}\ s^{-1}}. \quad (3)$$

The ERs emerging within a plage will undergo reconnection with the overlying AR loops. According to recent spectropolarimetric analyses of plage regions by Morosin et al. (2020), Pietrow et al. (2020), and Anan et al. (2021), the strength of the longitudinal field component in the chromosphere (at heights of up to ∼1 Mm, where the canopy has fully formed) is typically on the order of 400 G. Assuming that the field strength at the coronal base, B_0, is comparable to that in the upper chromosphere, we therefore normalize our estimates to $B_0 \sim 400$ G. The recycling time or timescale for an equal amount of minority-polarity flux to emerge under the plage field is given by

$$\tau_{\rm recyc} \sim \frac{B_0}{E_{\rm ER}(\Phi_{\rm ER} \gtrsim 1\times10^{18}\ {\rm Mx})/2} \sim 99\ {\rm hr}\ \left(\frac{B_0}{400\ {\rm G}}\right)\left[\frac{2.25\times10^{-3}\ {\rm Mx\ cm^{-2}\ s^{-1}}}{E_{\rm ER}(\Phi_{\rm ER} \gtrsim 1\times10^{18}\ {\rm Mx})}\right]. \quad (4)$$

Over this flux replacement time, all of the AR flux will have undergone reconnection with the ERs, with magnetic energy being dissipated in a layer whose thickness is determined by the heights of the ER loops. Denoting the average loop height by $\langle h_{\rm ER}\rangle$, we obtain for the energy flux density arising from footpoint reconnection:

$$F_{\rm ER} \sim \frac{B_0^2}{8\pi}\left(\frac{\langle h_{\rm ER}\rangle}{\tau_{\rm recyc}}\right) \sim 1.1\times10^{7}\ {\rm erg\ cm^{-2}\ s^{-1}}\left(\frac{B_0}{400\ {\rm G}}\right)\left(\frac{\langle h_{\rm ER}\rangle}{6.3\ {\rm Mm}}\right)\left[\frac{E_{\rm ER}(\Phi_{\rm ER} \gtrsim 1\times10^{18}\ {\rm Mx})}{2.25\times10^{-3}\ {\rm Mx\ cm^{-2}\ s^{-1}}}\right]. \quad (5)$$

Here, the average loop height has been normalized to the value corresponding to $\Phi_{\rm ER} = 1\times10^{19}$ Mx in Equation (2). The estimated energy flux density is close to the value of $\sim10^7$ erg cm^{-2} s^{-1} given by Withbroe and Noyes (1977) for the sum of the radiative and conductive energy losses in the AR corona.

The above estimate is based on the rate of ER emergence in the quiet Sun measured by Hagenaar et al. (2008, 2010). According to Figure 6 of Hagenaar et al. (2008), this rate and thus the recycling time are sensitive to the cadence of the magnetograms employed: as the interval Δt between successive magnetograms decreased from ∼1 hr to ∼5 minutes, $\tau_{\rm recyc}$ decreased from ∼13 to ∼1.5 hr. This raises the possibility that $E_{\rm ER}$ and thus $F_{\rm ER}$ would have been even larger had Hagenaar et al. used magnetograms taken less than 5 minutes apart. In the preceding section, we conjectured that ERs may have their origin in the churning of ubiquitous horizontal background fields by the solar granulation; if so, $\Delta t \sim 5$ minutes might turn out to be the appropriate timescale. However, this remains an important question that needs to be addressed by additional measurements.

The energy released in the reconnection events will be in the form of ohmic heating, jets, and MHD waves. The heat deposited near the coronal base is conducted both upward into the corona and downward through the transition region, with the resulting chromospheric evaporation acting to fill the AR loop with hot, dense material. We have here shown many examples of upflows, jets, and/or outward-propagating intensity fronts that originate from compact brightenings at the footpoints of AR loops. Winebarger et al. (2001) identified such upflows in TRACE 17.1 nm images of a bundle of loops in NOAA 8395, measuring projected speeds of 5–17 km s^{-1} for the intensity fronts. They conjectured that the flows were related to reconnection events, but found no evidence of flux cancellation in MDI magnetograms, presumably for the same reason(s) that the HMI magnetograms show no underlying minority-polarity flux in many of our examples.

As discussed by Warren et al. (2002, 2003), Winebarger et al. (2003), and Aschwanden et al. (2007), impulsive heating at the footpoints of AR loops also explains their orders-of-magnitude overdensity compared to that predicted by static loop models, the absence of significant temperature variations along the lengths of coronal loops (Lenz et al., 1999), as well as observations showing that loops initially appear at high temperatures before cooling to successively lower temperatures (see, e.g., Ugarte-Urra et al., 2006, 2009). The finding that the measured lifetimes of the loops are generally longer than their cooling timescales is consistent with AIA observations suggesting that a given AR loop may undergo a succession of interactions with the underlying small-scale features over periods of up to an hour or more (see, e.g., Figures 7–9).

Figure 1 in Wang et al. (2019) illustrates the evolution of an inverted-Y structure as observed in Fe IX 17.1 nm and Fe XIV 21.1 nm during 2013 April 30. The structure is rooted in a purely unipolar (according to the HMI magnetograms) plage area inside NOAA 11731. The outflow from the brightened, triangular base area is first seen in Fe XIV, and then in Fe IX after a lag of ∼10 minutes. Maintaining this time lag, both outflows reach their maximum intensity after ∼10 minutes and then fade more gradually over the next ∼20 minutes. Warren et al. (2002, 2003) modeled the evolution of TRACE loops observed simultaneously in the 17.1, 19.5, and 28.4 nm filters as involving multiple isothermal threads, with the threads having undergone impulsive footpoint heating at different times and being in different stages of cooling at any given time. Such a multi-thread model would be consistent with the complex topology expected of the small-scale footpoint fields as they are continually churned by granular motions and undergo reconnection with the overlying large-scale coronal field. The outflow example just described would suggest a well-defined onset time for the reconnection (perhaps associated with the emergence of an ER), followed by a succession of smaller events over a period of tens of minutes.

Reconnection between the AR loops and ER loops extending to heights $\gtrsim$2 Mm will also give rise to MHD waves originating near the coronal base. In the model of van Ballegooijen et al. (2011), a small fraction of the Alfvén waves generated by small-scale photospheric convective motions leaks into the corona; the waves are trapped inside the loop due to the steep gradients in the transition region at each end, interact with each other, and undergo turbulent dissipation. A similar scenario may apply if the Alfvén waves are generated by reconnection near the coronal base. Because the Alfvén crossing times in the corona are much shorter than the granular convection timescales on which the reconnection is driven, resonant interactions (not considered by van Ballegooijen et al.) may also occur between the trapped waves. However, in contrast to most models that invoke wave dissipation or nanoflares/braiding, we are here in a regime involving strongly antiparallel fields. We would thus expect the main energy release to be in the form of ohmic heating at the reconnection site, followed by heat conduction upward and downward along the coronal loop and the evaporation of material from the top of the chromosphere, as in solar flares.

5. Summary and Discussion

Although sometimes still advocated (see, e.g., Priest et al., 2018; Syntelis and Priest, 2020), reconnection with small-scale fields or the "magnetic carpet" appears to have fallen out of favor as a major coronal heating mechanism. Perhaps the main reason for this neglect is the near-absence of minority-polarity flux inside AR plages and strong network, according to even high-resolution magnetograms. This study provides additional support for our earlier conclusion that present-day magnetograms greatly underestimate the amount of minority-polarity flux at the footpoints of AR loops (Wang, 2016; Wang et al., 2019), and suggests that the reconnection rate is sufficient to heat the AR corona. The failure to detect the minority-polarity flux may indicate a problem with instrument sensitivity when one polarity is heavily dominant and the minority-polarity signal is close to the nominal $\sim$10 G noise level.

One of the important points made here (see, e.g., Figures 2 and 10) and in our previous studies is that the spatial distribution and morphological appearance of looplike fine structure in 17.1 and 19.3 nm images seem to be the same inside and just outside "unipolar" regions. This absence of a well defined boundary for the "moss" leads us to infer that the rate of small-scale flux emergence (or churning of small-scale fields by granular convection) is similar everywhere on the Sun, irrespective of the local degree of unipolarity.

Taking the emergence rate to be the same as that measured by Hagenaar et al. (2008, 2010) for ERs outside of unipolar areas, we have estimated the energy flux density due

to reconnection with plage fields, $F_{\rm ER}$, to be on the order of 10^7 erg cm^{-2} s^{-1}, enough to account for the heating of the AR corona. In general, $F_{\rm ER} \propto (B_0^2/8\pi)/\tau_{\rm recyc} \propto B_0$, where B_0 is the field strength at the coronal base and $\tau_{\rm recyc} \propto B_0$ is the timescale for all of the flux to undergo reconnection with ERs. Inside coronal holes, where $B_0 \sim 10$ G instead of ∼300–400 G, $F_{\rm ER} \sim 3 \times 10^5$ erg cm^{-2} s^{-1}, which is sufficient to heat the hole and drive the solar wind. Using energy conservation along a flux tube and tracing from Earth back to the solar surface, we have verified that the observed solar-wind energy flux density (which is dominated at 1 au by the kinetic energy of the bulk flow, $\rho v^3/2$) is indeed proportional to the field strength at the coronal base (Wang, 2010, 2020).

Although we have been concerned here only with the heating of the corona, it may be that mixed-polarity flux on even smaller scales plays an important part in chromospheric heating, given the power law distribution of flux emergence. In their high-resolution spectropolarimetric study of chromospheric heating in a plage region, Anan et al. (2021) found that the Mg II radiative flux (a measure of the heating rate) was highest in between or at the edges of the individual strong field patches within the plage, and was poorly correlated with the local chromospheric or photospheric field strength. Reconnection with small bipoles scattered through the plage might account for such off-center heating.

Our key prediction is that, rather than simply representing the transition region of hot AR loops, "moss" actually contains small loops that undergo continual interactions with the overlying coronal loops and are responsible for their heating. The *Extreme Ultraviolet Imager* and the *Polarimetric and Helioseismic Imager* on *Solar Orbiter* may soon provide an opportunity to test this prediction. In addition, we anticipate that the *Daniel K. Inouye Solar Telescope*'s spectropolarimeters, with their unprecedented sensitivity and spatial resolution, will help us to understand better the nature of the plage fields.

We thank J. M. Laming for discussions. This work was supported by NASA and the Office of Naval Research.

REFERENCES

Abramenko, V. I., Fisk, L. A., Yurchyshyn, V. B.: 2006, *Astrophys. J. Lett.* **641,** L65.

Anan, T., Schad, T. A., Kitai, R., Dima, G. I., Jaeggli, S. A., Tarr, L. A., Collados, M., Dominguez-Tagle, C., Kleint, L.: 2021, *Astrophys. J.* **921,** 39.

Aschwanden, M. J., Winebarger, A., Tsiklauri, D., Peter, H.: 2007, *Astrophys. J.* **659,** 1673.

Berger, T. E., De Pontieu, B., Schrijver, C. J., Title, A. M.: 1999, *Astrophys. J. Lett.* **519,** L97.

Berghmans, D., Auchère, F., Long, D. M., Soubrié, E., Mierla, M., Zhukov, A. N., Schühle, U., Antolin, P., Harra, L., Parenti, S., Podladchikova, O., Aznar Cuadrado, R., Buchlin, É., Dolla, L., Verbeeck, C., Gissot, S., Teriaca, L., Haberreiter, M., Katsiyannis, A. C., Rodriguez, L., Kraaikamp, E., Smith, P. J., Stegen, K., Rochus, P., Halain, J. P., Jacques, L., Thompson, W. T., Inhester, B.: 2021, *Astron. Astrophys.* **656**, L4.

Chitta, L. P., Peter, H., Solanki, S. K., Barthol, P., Gandorfer, A., Gizon, L., Hirzberger, J., Riethmüller, T. L., van Noort, M., Blanco Rodríguez, J., Del Toro Iniesta, J. C., Orozco Suárez, D., Schmidt, W., Martínez Pillet, V., Knölker, M.: 2017, *Astrophys. J. Suppl. Ser.* **229,** 4.

Cranmer, S. R., van Ballegooijen, A. A.: 2005, *Astrophys. J. Suppl. Ser.* **156,** 265.

Cranmer, S. R., van Ballegooijen, A. A.: 2010, *Astrophys. J.* **720,** 824.

Dahlburg, R. B., Einaudi, G., Taylor, B. D., Ugarte-Urra, I., Warren, H. P., Rappazzo, A. F., Velli, M.: 2016, *Astrophys. J.* **817,** 47.

De Groof, A., Goossens, M.: 2002, *Astron. Astrophys.* **386,** 691.

De Pontieu, B., Berger, T. E., Schrijver, C. J., Title, A. M.: 1999, *Solar Phys.* **190,** 419.

De Pontieu, B., Hansteen, V. H., McIntosh, S. W., Patsourakos, S.: 2009, *Astrophys. J.* **702,** 1016.

De Pontieu, B., Tarbell, T., Erdélyi, R.: 2003, *Astrophys. J.* **590,** 502.

Fisk, L. A.: 2005, *Astrophys. J.* **626,** 563.

Hagenaar, H. J.: 2001, *Astrophys. J.* **555,** 448.

Hagenaar, H. J., DeRosa, M. L., Schrijver, C. J.: 2008, *Astrophys. J.* **678,** 541.

Hagenaar, H. J., DeRosa, M. L., Schrijver, C. J.: 2010, *Astrophys. J.* **715,** 696.

Hagenaar, H. J., Schrijver, C. J., Title, A. M.: 2003, *Astrophys. J.* **584,** 1107.

Hale, G. E., Ellerman, F.: 1903, *Publ. Yerkes Obs.* **3,** 3.

Hansteen, V. H., De Pontieu, B., Rouppe van der Voort, L., van Noort, M., Carlsson, M.: 2006, *Astrophys. J. Lett.* **647,** L73.

Harvey, J. W., Branston, D., Henney, C. J., Keller, C. U.: 2007, *Astrophys. J. Lett.* **659,** L177.

Howard, R., Harvey, J. W.: 1964, *Astrophys. J.* **139,** 1328.

Howson, T. A., De Moortel, I., Antolin, P., Van Doorsselaere, T., Wright, A. N.: 2019, *Astron. Astrophys.* **631,** A105.

Lenz, D. D., DeLuca, E. E., Golub, L., Rosner, R., Bookbinder, J. A.: 1999, *Astrophys. J. Lett.* **517,** L155.

Lites, B. W., Leka, K. D., Skumanich, A., Martínez Pillet, V., Shimizu, T.: 1996, *Astrophys. J.* **460,** 1019.

Morosin, R., de la Cruz Rodríguez, J., Vissers, G. J. M., Yadav, R.: 2020, *Astron. Astrophys.* **642,** A210.

Parker, E. N.: 1988, *Astrophys. J.* **330,** 474.

Parker, E. N.: 1991, *Astrophys. J.* **372,** 719.

Parnell, C. E., De Moortel, I.: 2012, *Phil. Trans. Roy. Soc. London Ser. A* **370,** 3217.

Pietrow, A. G. M., Kiselman, D., de la Cruz Rodríguez, J., Díaz Baso, C. J., Pastor Yabar, A., Yadav, R.: 2020, *Astron. Astrophys.* **644,** A43.

Pontin, D. I., Hornig, G.: 2020, *Liv. Rev. Solar Phys.* **17,** 5.

Priest, E. R., Chitta, L. P., Syntelis, P.: 2018, *Astrophys. J. Lett.* **862,** L24.

Schrijver, C. J., Title, A. M., Harvey, K. L., Sheeley, N. R., Jr., Wang, Y.-M., van den Oord, G. H. J., Shine, R. A., Tarbell, T. D., Hurlburt, N. E.: 1998, *Nature* **394,** 152.

St. John, C. E.: 1911, *Astrophys. J.* **34,** 57.

Syntelis, P., Priest, E. R.: 2020, *Astrophys. J.* **891,** 52.

Thornton, L. M., Parnell, C. E.: 2011, *Solar Phys.* **269,** 13.

Tran, T., Bertello, L., Ulrich, R. K., Evans, S.: 2005, *Astrophys. J. Suppl. Ser.* **156,** 295.

Tsiropoula, G., Tziotziou, K.: 2004, *Astron. Astrophys.* **424,** 279.

Ugarte-Urra, I., Warren, H. P, Brooks, D. H.: 2009, *Astrophys. J.* **695,** 642.

Ugarte-Urra, I., Winebarger, A. R., Warren, H. P.: 2006, *Astrophys. J.* **643,** 1245.

van Ballegooijen, A. A., Asgari-Targhi, M., Berger, M. A.: 2014, *Astrophys. J.* **787,** 87.

van Ballegooijen, A. A., Asgari-Targhi, M., Cranmer, S. R., DeLuca, E. E.: 2011, *Astrophys. J.* **736,** 3.

Wang, Y.-M.: 2010, *Astrophys. J. Lett.* **715,** L121.

Wang, Y.-M.: 2016, *Astrophys. J. Lett.* **820,** L13.

Wang, Y.-M.: 2020, *Astrophys. J.* **904,** 199.

Wang, Y.-M., Berger, M. A.: 2018, *Astrophys. J.* **868,** 66.

Wang, Y.-M., Robbrecht, E., Muglach, K.: 2011, *Astrophys. J.* **733,** 20.

Wang, Y.-M., Ugarte-Urra, I., Reep, J. W.: 2019, *Astrophys. J.* **885,** 34.

Wang, Y.-M., Warren, H. P., Muglach, K.: 2016, *Astrophys. J.* **818,** 203.

Warren, H. P., Winebarger, A. R., Hamilton, P. S.: 2002, *Astrophys. J. Lett.* **579,** L41.

Warren, H. P., Winebarger, A. R., Mariska, J. T.: 2003, *Astrophys. J.* **593,** 1174.

Winebarger, A. R., DeLuca, E. E., Golub, L.: 2001, *Astrophys. J. Lett.* **553,** L81.

Winebarger, A. R., Warren, H. P., Seaton, D. B.: 2003, *Astrophys. J.* **593,** 1164.

Withbroe, G. L., Noyes, R. W.: 1977, *Annu. Rev. Astron. Astrophys.* **15,** 363.

Zhang, J., Ma, J., Wang, H.: 2006, *Astrophys. J.* **649,** 464.

Zhou, G., Wang, J., Jin, C.: 2013, *Solar Phys.* **283,** 273.

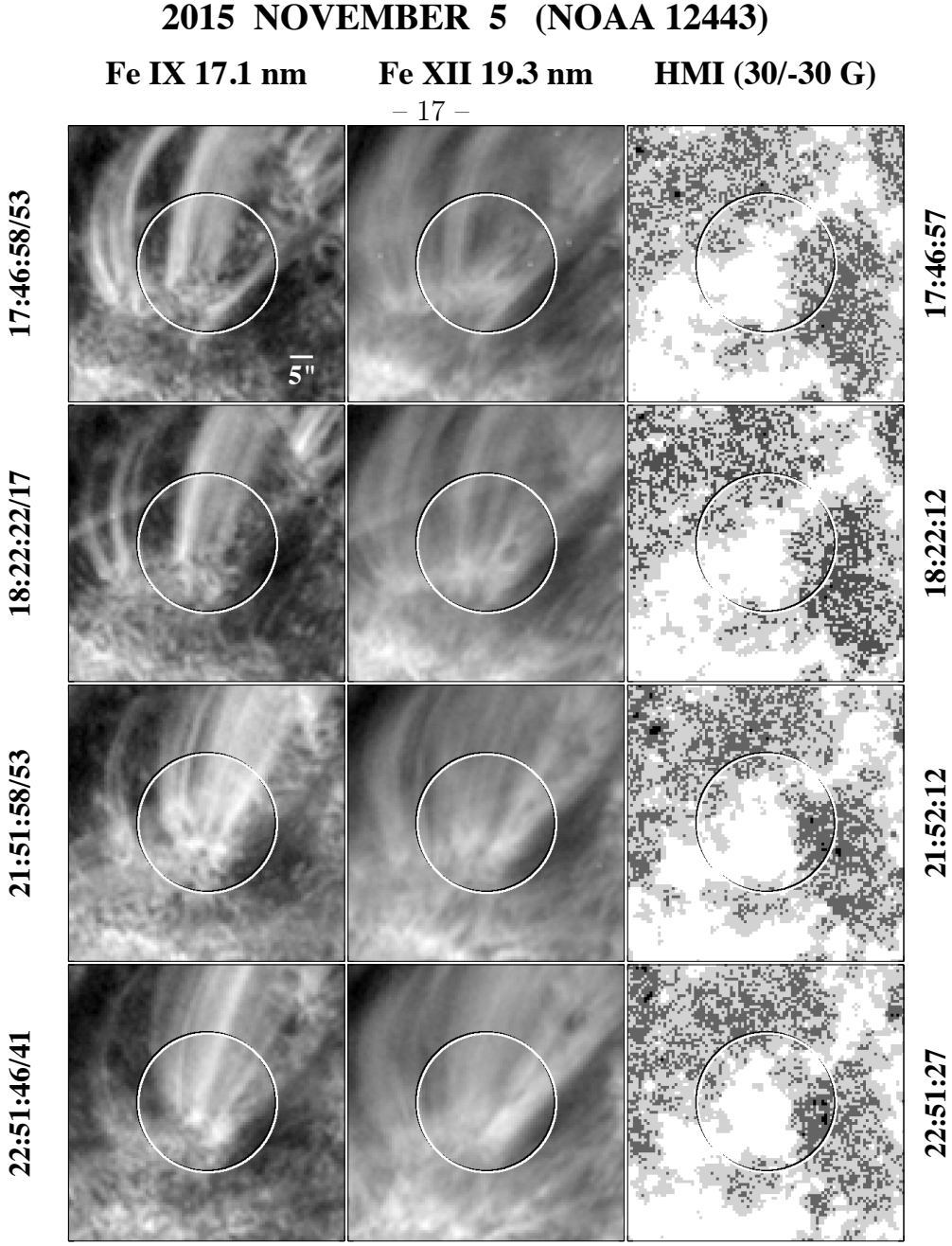

Fig. 1.— A cluster of coronal loops observed inside NOAA 12443 late on 2015 November 5. Circled area has radius 15″. The Fe IX 17.1 nm (left column) and Fe XII 19.3 nm (middle column) loops are rooted in moss overlying a plage area containing only positive-polarity flux, according to the corresponding HMI magnetograms (right column). The brightness and spatial distribution of the 17.1 nm loops vary continually over the 5 hr period, as does the underlying fine structure, which, in addition to dark chromospheric material, consists of looplike features and compact brightenings that appear to be an integral part of the moss. The emission is more diffuse and widespread in the 19.3 nm images (recorded 5 s before the 17.1 nm images), but the brightenings are still visible at the loop footpoints. Movies suggest that the fading of the Fe IX loops is often accompanied by downflows (see the animation accompanying Figure 10 in Wang et al., 2019). Here and in subsequent figures, the gray scale used in the magnetograms is as follows: white ($B_{\rm los} > 30$ G); light gray (0 G $< B_{\rm los} <$ 30 G); dark gray (-30 G $< B_{\rm los} < 0$ G); black ($B_{\rm los} < -30$ G).

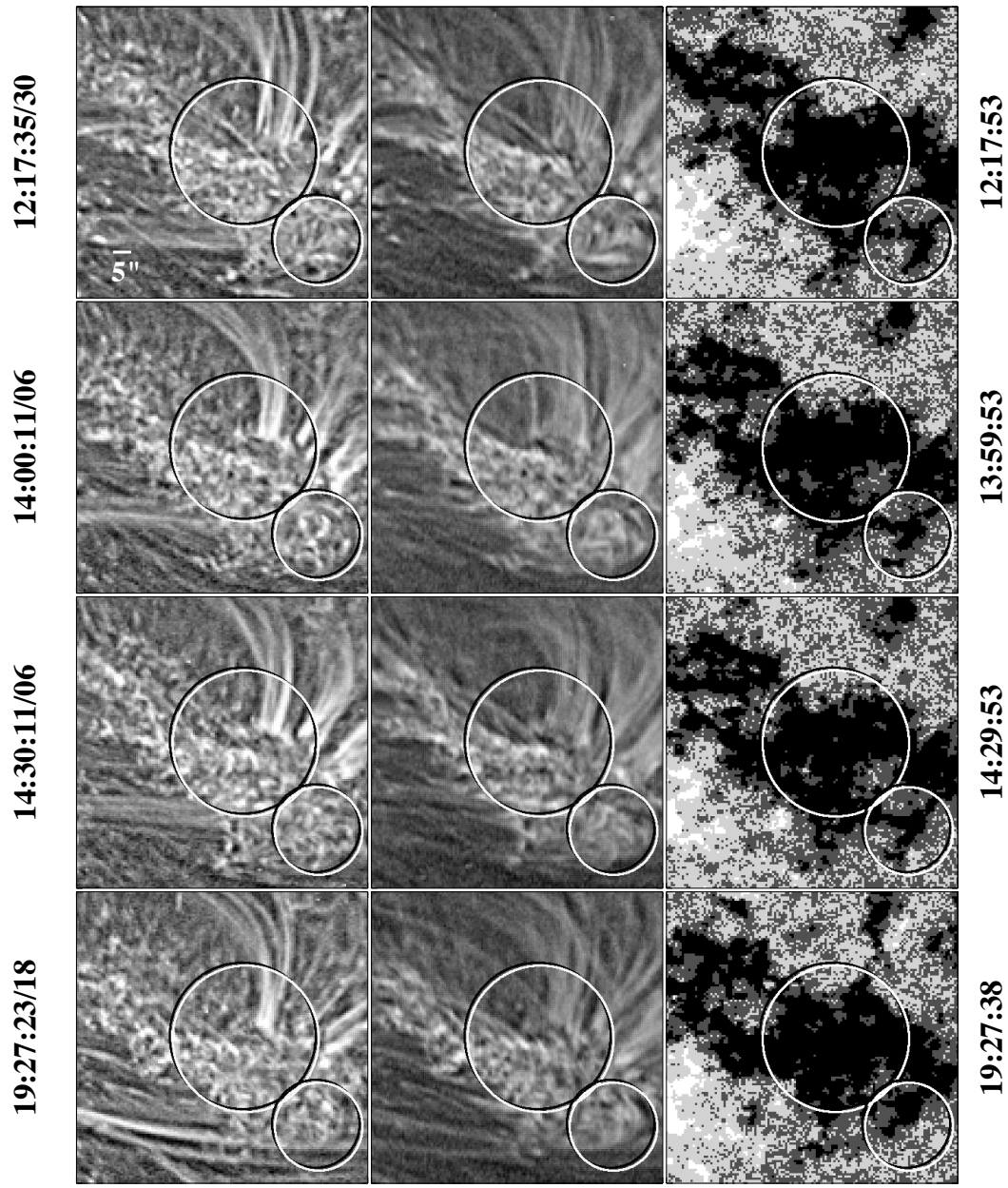

Fig. 2.— Small loop-shaped features embedded within the moss/plage inside NOAA 12351, as observed on 2015 May 23. Left column: Fe IX 17.1 nm images recorded at 12:17:35, 14:00:11, 14:30:11, and 19:27:23 UTC. Middle column: Fe X11 19.3 nm images recorded at 12:17:30, 14:00:06, 14:30:06, and 19:27:18 UTC. Right column: line-of-sight HMI magnetograms recorded at 12:17:53, 13:59:53, 14:29:53, and 19:27:38 UTC and saturated at ±30 G. An unsharp mask has been applied to the EUV images. Note that the moss-like structure and looplike features extend into the mixed-polarity, weaker-field areas beyond the plage itself, as indicated for example by the circled region at the southwest corner of the images. Loop-shaped structures with dimensions of a few arcseconds may be discerned not only in Fe IX but also in Fe XII, as near the center of the large circles in the 19.3 nm images taken at 14:00 and 14:30 UTC.

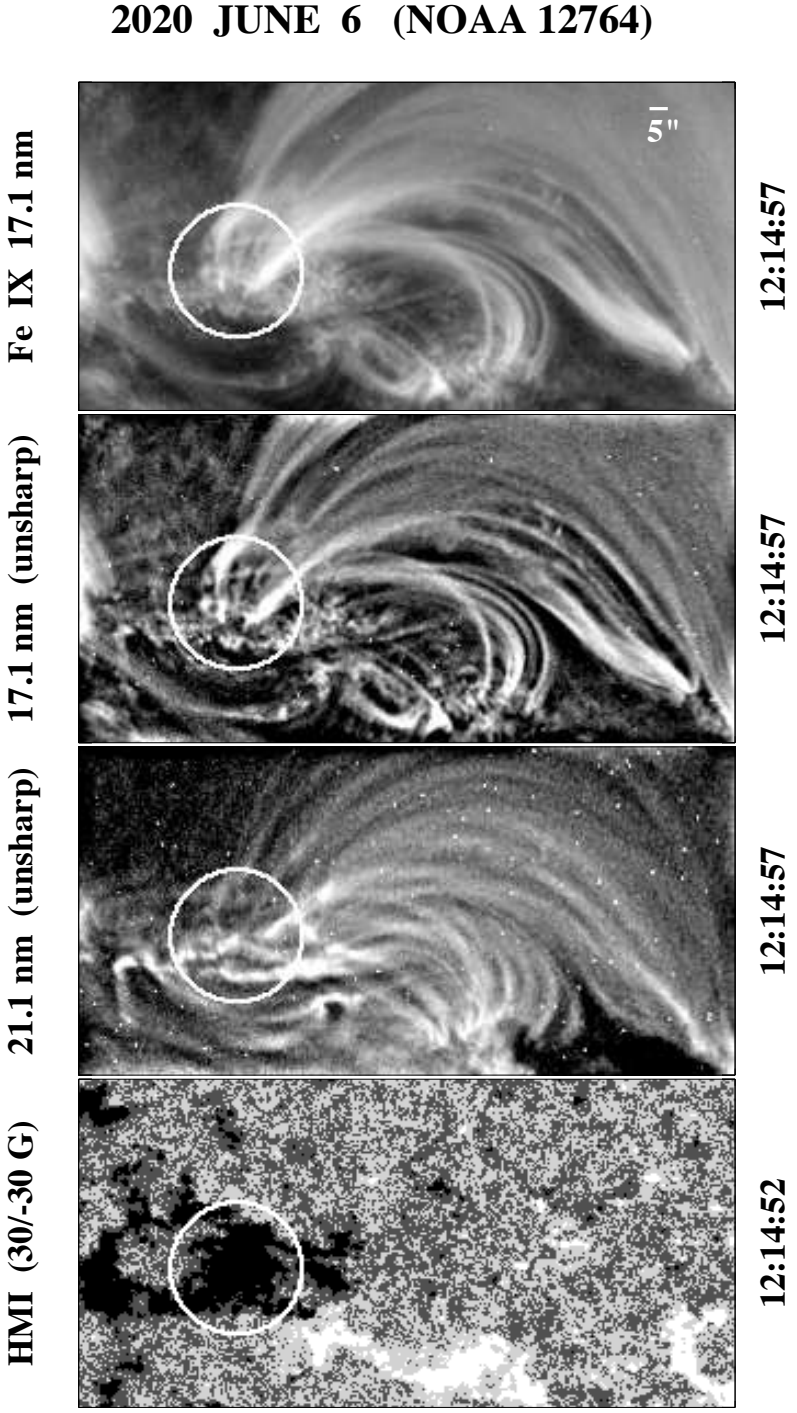

Fig. 3.— AR loop system (NOAA 12764) observed on 2020 June 6, at the onset of solar cycle 25. Within the circled area (of radius 18″), looplike features with dimensions on the order of 5″ may be seen at the footpoints of the longer loops. These features are embedded in the 17.1 nm moss overlying the negative-polarity plage.

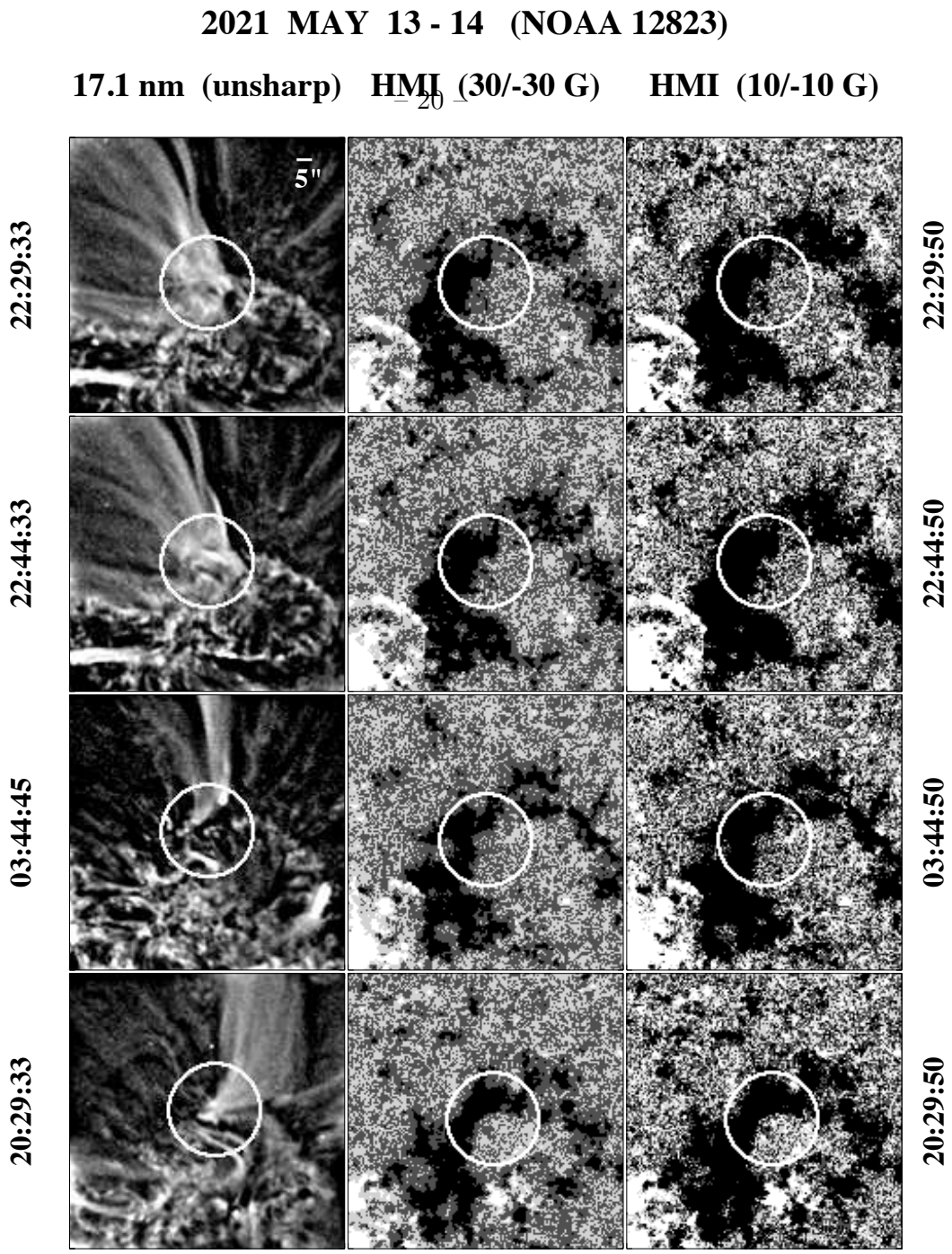

Fig. 4.— Evolution of 17.1 nm loops inside NOAA 12823, 2021 May 13–14. As the underlying plage area narrows, the cluster of AR loops present late on May 13 fades and is replaced by a smaller bundle on May 14. Relatively large ($\gtrsim 5''$) looplike features may be seen at the base of the AR loops; some of these footpoint structures have at least one leg located above the weak, mixed-polarity region on the west side of the negative-polarity plage. The magnetograms in the rightmost column have been saturated at ± 10 G instead of ± 30 G (as in the middle column), so that light and dark gray pixels here indicate locations where $B_{\rm los}$ is close to the HMI noise level.

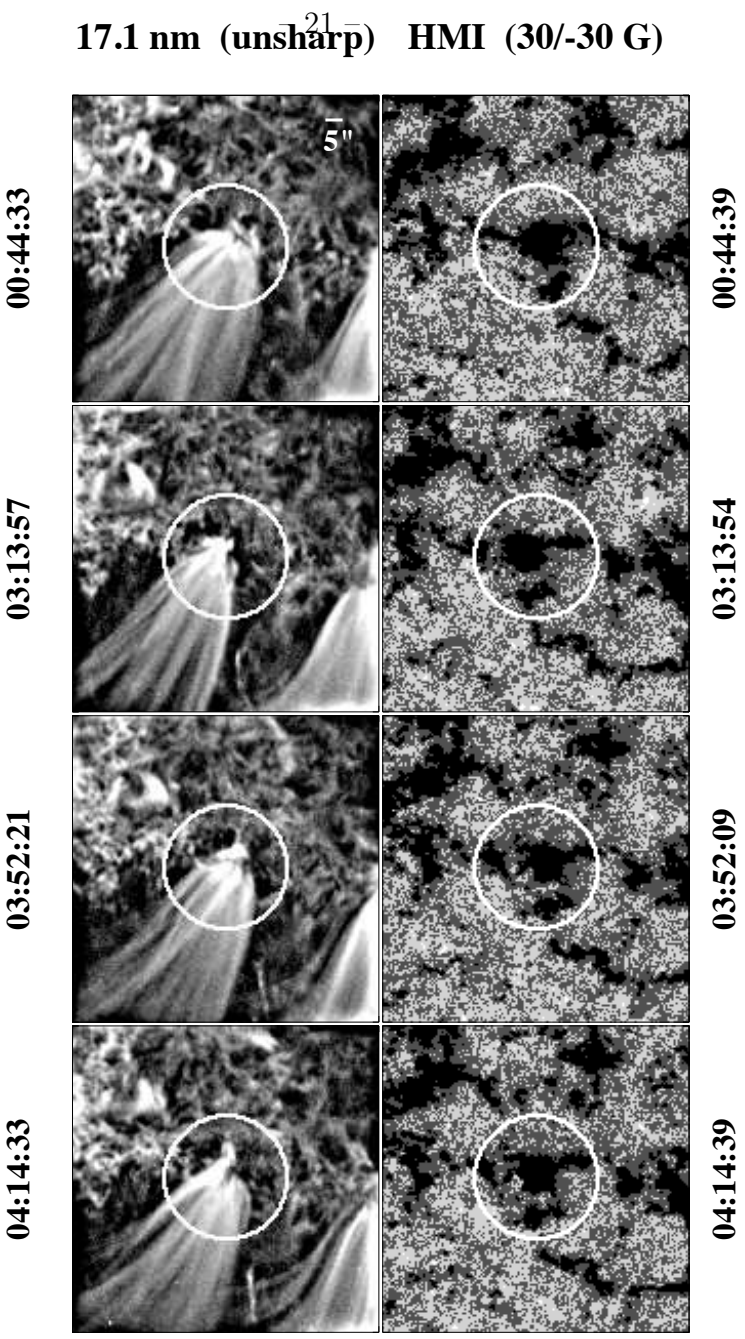

Fig. 5.— The western end of a bundle of 17.1 nm loops is here viewed "from above." The loops are rooted in a fragment of negative-polarity plage on the west side of NOAA 12783, 2020 November 21. Small, bright features may be seen at the terminus of the loops, some of which are embedded within the unipolar plage.

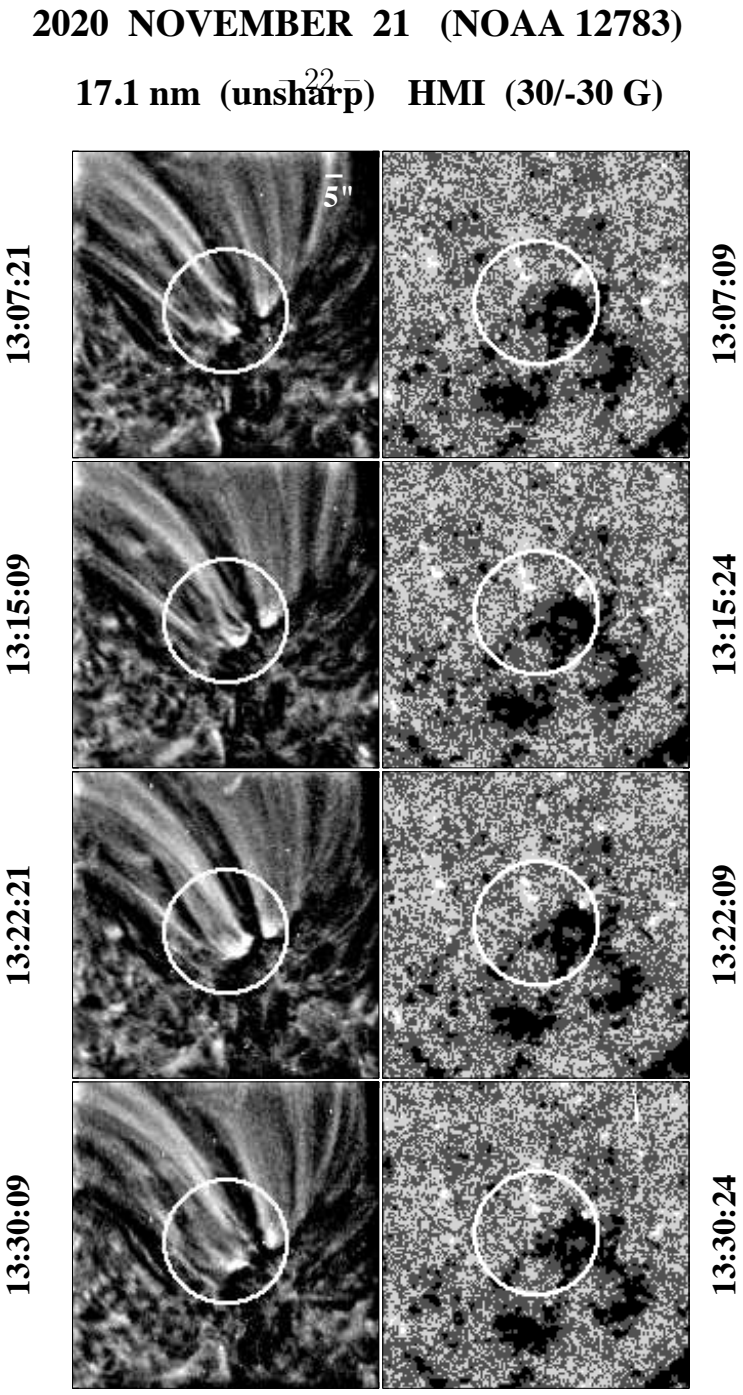

Fig. 6.— Compact brightenings at the footpoints of 17.1 nm loops, as observed near the northwestern edge of NOAA 12783 on 2020 November 21. The intensities and spatial distribution of the footpoint brightenings, some of which are accompanied by jets or narrow outflows along the overlying loops, vary continually on timescales of minutes.

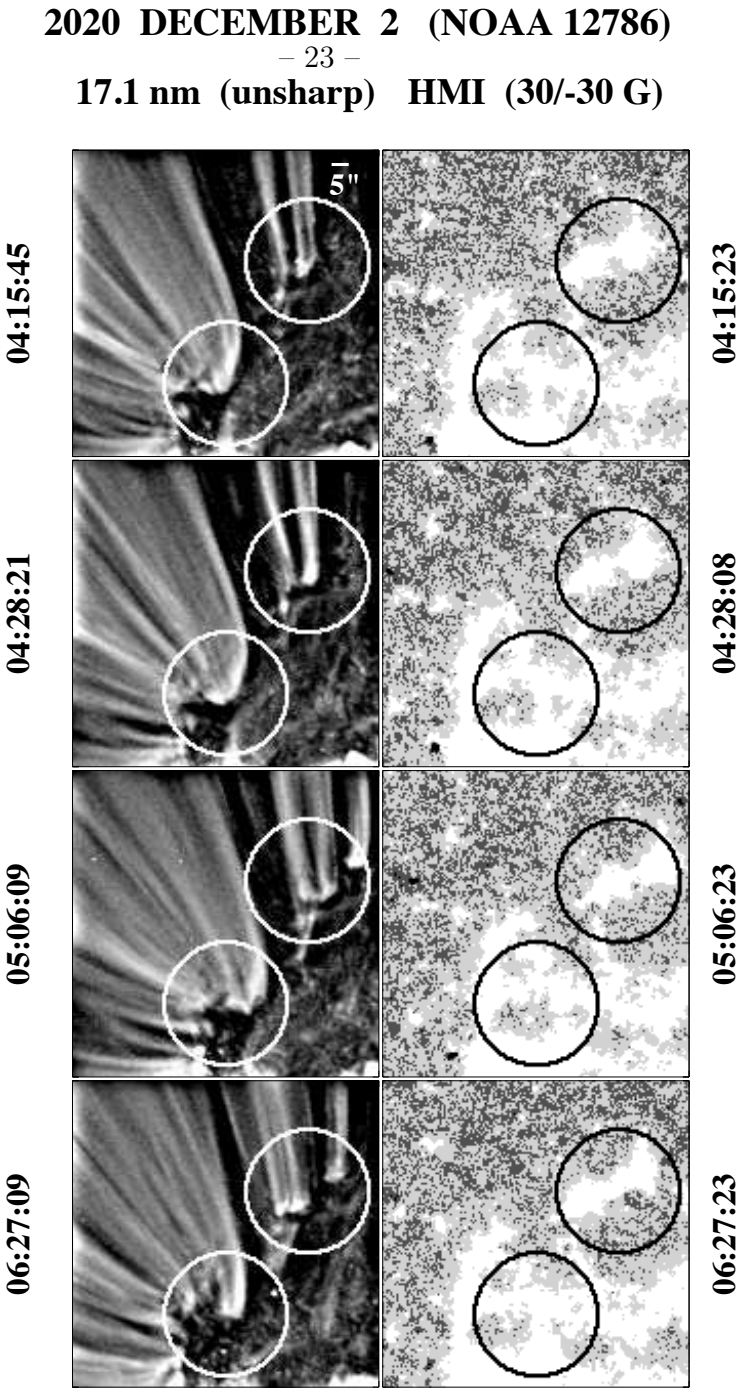

Fig. 7.— More examples of 17.1 nm AR loops with compact brightenings at their bases. The loops in this case are rooted in and around a unipolar plage area inside NOAA 12786. Again, bright jet-like outflows may be seen emanating from many of the footpoint features.

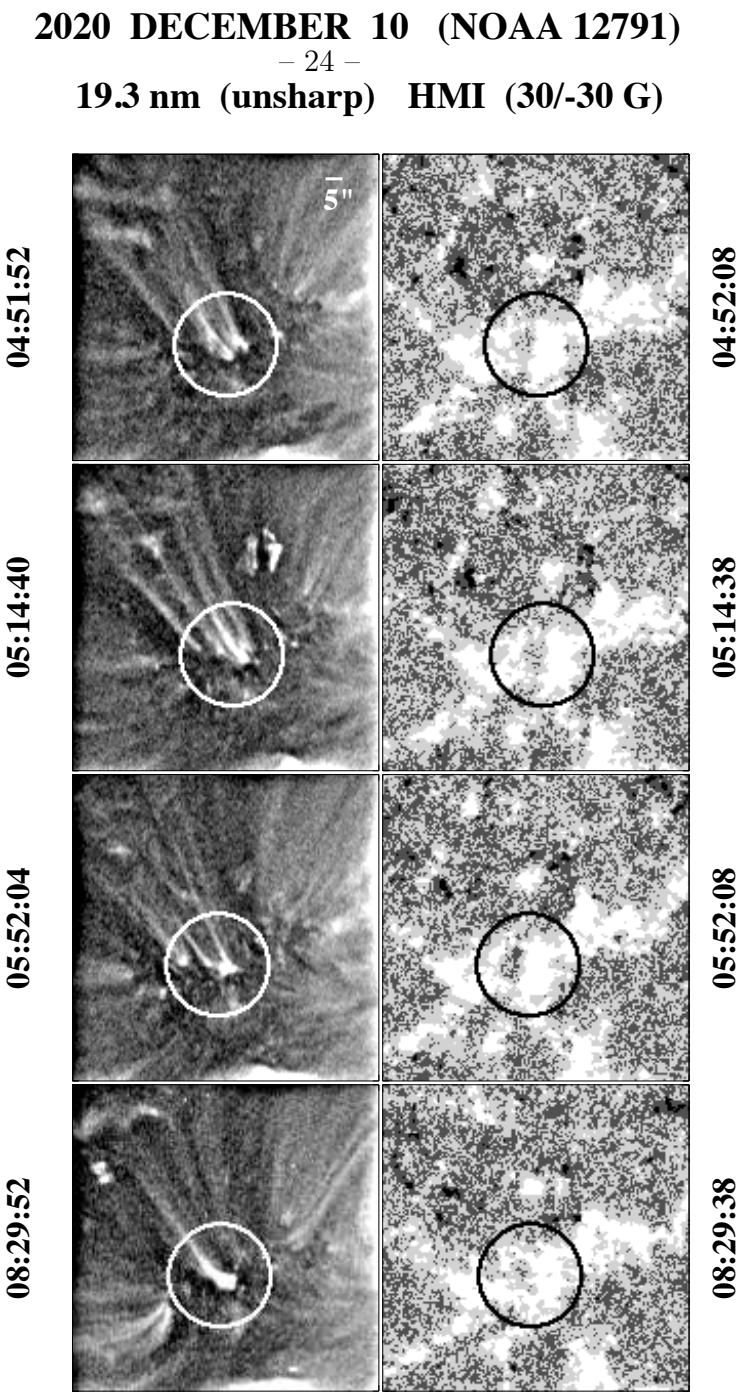

Fig. 8.— Compact brightenings at the footpoints of Fe XII 19.3 nm loops in NOAA 12791, 2020 December 10. Again, the footpoint brightenings are accompanied by jet-like outflows, and some of the compact features appear to be embedded in purely unipolar flux.

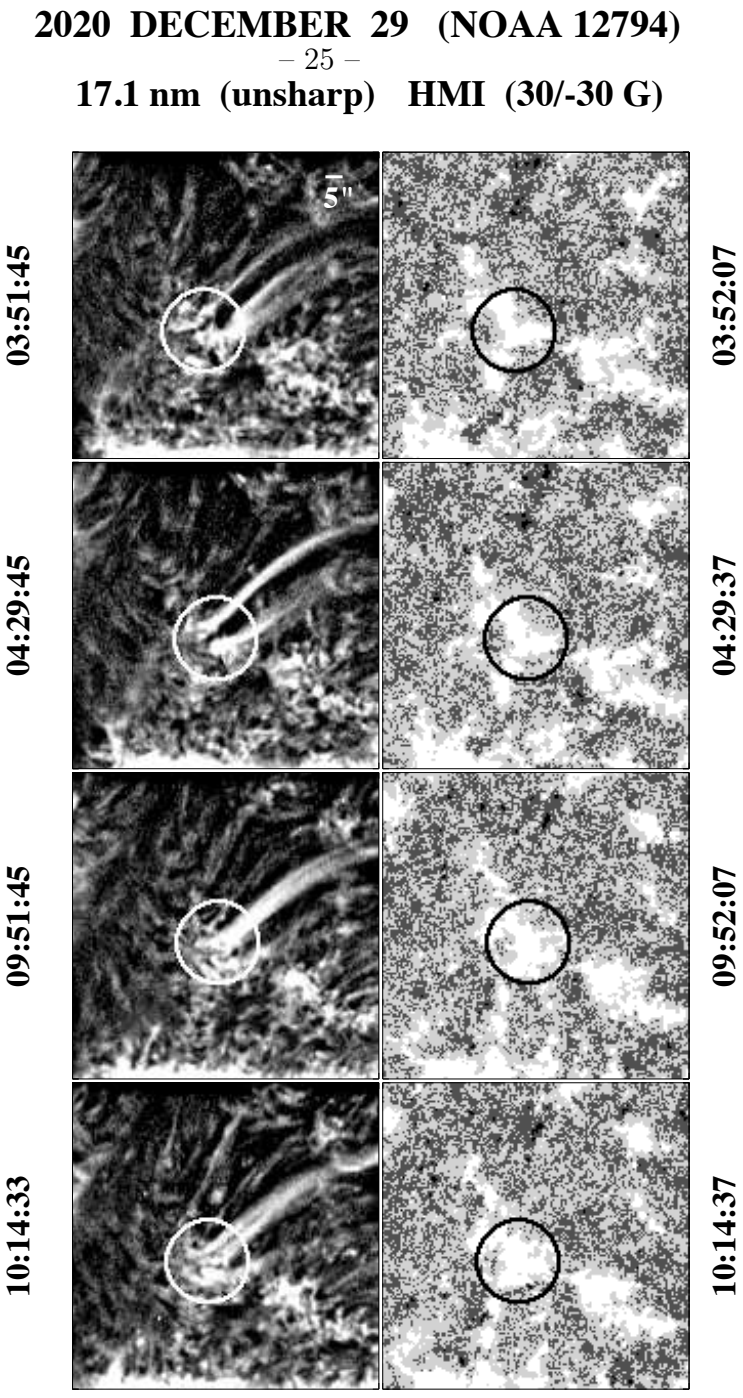

Fig. 9.— The highly time-varying 17.1 nm outflows seen here are directed toward a large, negative-polarity sunspot in NOAA 12794. Note the complex fine structure at the bases of the loops.

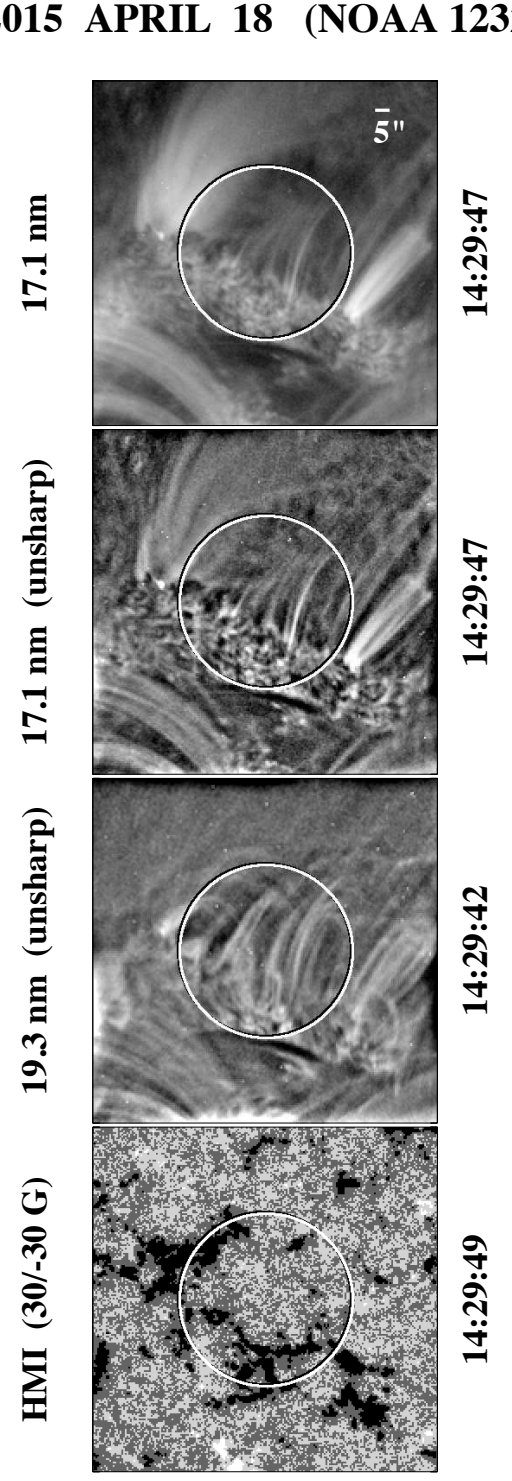

Fig. 10.— An example of 17.1 nm "moss" overlying an area of relatively weak photospheric field. The obvious presence of mixed-polarity flux in this case supports the idea that small loops are a major constituent of moss, including that observed in "unipolar" plage areas. (See also Figure 2, where the small circles highlight moss- and looplike structure extending beyond the edge of the plage.)